

Principal Component Global Analysis of Series of Fluorescence Spectra

Wajih Al-Soufi, Mercedes Novo, Manuel Mosquera,
and Flor Rodríguez-Prieto

Abstract The analysis of series of molecular fluorescence or absorption spectra forms an integral part of innumerable investigations on the physicochemical properties of chemical or biological systems.

In many typical complex applications, such as photochemical systems with multiple interconversion processes in the ground and in the excited states or biochemical ligand binding studies with several possible binding sites, the number of species contributing to the spectral variation is not known a priori. Moreover, in the frequent case of strongly overlapping spectra of the species, their number cannot be estimated by simple inspection of the experimental spectra.

Principal Component Global Analysis (PCGA) is reviewed as an efficient and reliable way to determine how many species contribute to the observed spectral variation, to set up the correct mechanism and to estimate the values of the corresponding model-parameters. PCGA is applied to examples of host-guest interactions with two and three components and to systems showing complex ground and excited-state proton-transfer reactions with corresponding one and two acid-base equilibria.

1 Introduction

Analysis of series of molecular fluorescence or absorption spectra forms an integral part of innumerable investigations on the physicochemical properties of chemical or biological systems. The detailed analysis of the variation observed in these spectra by changing systematically an externally controllable variable such as pH, concentration, temperature, or time reveals the nature of the contributing species

W. Al-Soufi (✉)

Departamento de Química Física, Facultade de Ciencias, Universidade de Santiago de Compostela, E-27002 Lugo, Spain
e-mail: wajih.al-soufi@usc.es

and leads to a full understanding of the underlying reaction mechanisms and the corresponding equilibrium or kinetic constants.

In many typical complex applications, such as photochemical systems with multiple interconversion processes in the ground and in the excited states or biochemical ligand binding studies with several possible binding sites, the number of species contributing to the spectral variation is not known *a priori*. Moreover, in the frequent case of strongly overlapping spectra of the species, their number cannot be estimated by simple inspection of the experimental spectra.

Two main questions arise in these studies. First: how many species contribute to the observed spectral variation? And second: which is the correct mechanism and what are the values of the corresponding model parameters that best reproduce the spectra?

Classically both problems are tackled together making hypothesis on both the *number* of species and the underlying *model* and then testing the two hypothesis in one step, fitting the model to the experimental data at a single (or few) wavelengths with least-squares algorithms. On the basis of the quality of the resulting fit, the tested hypothesis is accepted or rejected. This can be a tedious task, since the answer to how many species contribute relies itself on the validity of the proposed model. Moreover, a model which works well at single wavelengths may fail to reproduce the full spectra. A correct model should describe the observed spectra in the whole accessible spectral interval with the same set of parameter values.

The answers to these questions are not trivial and in spite of innumerable publications relying on the interpretation of series of fluorescence spectra, there is no broad acceptance of a systematic solution.

In this contribution, we review principal component global analysis (PCGA) as an efficient and reliable way to get answers to these questions and present briefly the theory and typical applications.

PCGA separates the determination of the *number* of contributing components from the test and fit of different *models* to the data. In a first step, the series of experimental spectra is reduced by principal component analysis (PCA) to the *minimal* number of “abstract spectra” (eigenvectors), which reproduce all the systematic change in the original spectra. This yields the number of contributing components. In a second step, this information is used in a global analysis to test different model functions and to find estimates for the model parameters and the component spectra. In this step, the model functions are globally fitted to all spectra at *all* available wavelengths simultaneously. This approach allows one to estimate the emission spectra of contributing species from strongly overlapping spectra, which would be otherwise very difficult to determine if they cannot be experimentally isolated. Moreover, from the component spectra, important information can be derived, for example, the relative quantum efficiencies comparing spectral areas.

In the chemometric literature, many related analytical methods have been described, such as “window factor analysis” (WFA) [16], “self modeling curve resolution” [10, 25, 26, 28, 29], “second order global analysis” [9], and others. A comprehensive tutorial was published only recently on the analysis of reaction kinetic data [22].

In physical chemistry, the interest is focused mostly on the validation of different complex mechanisms which are generally not accessible to standardized solutions. Systems such as the lactim–lactam phototautomerization presented in Sect. 5.3 with multiple coupled equilibria and a complex dependence on the solvent proton concentration need careful and stepwise identification of the contributing species and a systematic resolution and validation of the underlying mechanism, combining information from different spectroscopic techniques and comparing results obtained in different solvents.

2 Example System

We illustrate the application of PCGA with typical physicochemical systems which depend on different external parameters: two examples of host–guest interactions with two and three components and two systems showing complex ground and excited-state proton-transfer reactions with corresponding one and two acid–base equilibria. The theory is accompanied with the results for the two component host–guest association equilibrium between the fluorescent dye Pyronine Y as guest and β -cyclodextrin as host. The results for the other example systems are explained in Chap. 5. More examples can be found in the literature [5, 15, 24].

2.1 Host–Guest Interaction Between Pyronine Y and β -Cyclodextrin

Small guests such as the fluorescent dye Pyronine Y (PY) can form inclusion complexes with β -cyclodextrin (CD), a toroidally shaped polysaccharide with a highly hydrophobic central cavity. Complexation induces significant changes in the physicochemical properties of PY and the stoichiometry of the complexes can be determined from titration experiments measuring series of absorption and emission spectra of the dye in the presence of different concentrations of CD. From these spectra the number of different species present in solution can be determined with PCA. GA confirms then the stoichiometry and yields the association equilibrium constants and the pure spectra of the species [23].

Figure 1 shows a series of $n_s = 22$ emission spectra from titration experiments. Red shift of the spectra together with a decrease in fluorescence intensity is observed as the concentration of CD is increased. The number of emitting species is not obvious from these data and has to be determined by further analysis such as PCGA as presented in the following section.

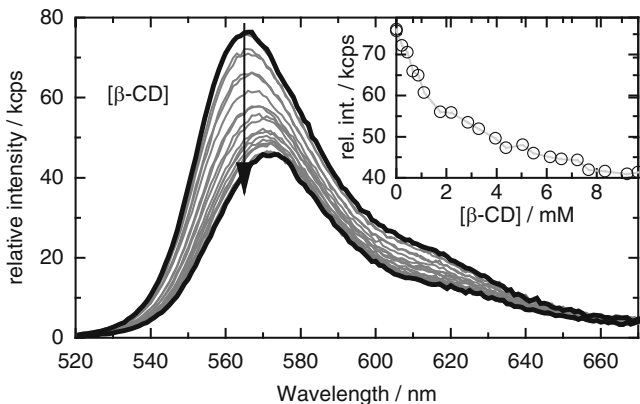


Fig. 1 Corrected fluorescence emission spectra of PY in the presence of different concentrations of β -CD in the range from 1×10^{-5} to 9.7×10^{-3} mol dm $^{-3}$ ($\lambda_{\text{exc}} = 515$ nm, $n_w = 150$, $n_s = 22$). *Inset*: Intensity profile vs. β -CD concentration at 565 nm

3 Determination of the Number of Fluorescent Species by Principal Component Analysis

Principal component analysis (PCA) and the related factor analysis are well-known, validated statistical techniques, widely used in different areas of experimental science [12, 17]. Their application for dimensionality reduction, classification, regression, etc. is described extensively in the chemometric literature and PCA forms part of many statistical software packages. However, in spite of its widespread use in analytical chemistry, PCA has been rarely applied in physicochemical studies. This is especially surprising as the determination of the number of fluorescent species from series of emission spectra with PCA is straightforward and very efficient. The procedure is easily programmed in modern mathematical packages and can form part of routine data analysis.

We will give here a concise introduction to the key equations with the data from Sect. 2.1 as example.

PCA can be applied to any series of spectra which are *linear* combinations of a set of *constant* “component spectra” with relative contributions which depend on some “external” variable such as pH, concentration of a ligand or reaction partner, temperature, or time. In this case, the i th experimental spectrum, y_i , is the sum of n_c component spectra e_j , weighted with contributions (concentrations) d_{ij} plus some noise σ_i :

$$y_i = d_{i1}e_1 + d_{i2}e_2 + \cdots + d_{in_c}e_{n_c} + \sigma_i = \hat{y}_i + \sigma_i. \quad (1)$$

The spectral data can be arranged in an experimental data matrix \mathbf{Y} with the rows containing the spectra and the columns reproducing the variation of

the emission at one wavelength with the external variable. In matrix notation, the matrix of the theoretical spectra $\hat{\mathbf{Y}}$ is the product of the matrix of component spectra \mathbf{E} with the matrix of concentrations \mathbf{D} which depend on some model and on the “external” variable:

$$\begin{aligned} \hat{\mathbf{Y}}_{n_s \times n_w} &= \begin{pmatrix} \hat{y}_{1,1} & \cdots & \hat{y}_{1,n_w} \\ \vdots & \ddots & \vdots \\ \hat{y}_{n_s,1} & \cdots & \hat{y}_{n_s,n_w} \end{pmatrix} = \underset{n_s \times n_c}{\mathbf{D}} \cdot \underset{n_c \times n_w}{\mathbf{E}} \\ &= \begin{pmatrix} d_{1,1} & \vdots & d_{1,n_c} \\ \vdots & \vdots & \vdots \\ d_{n_s,1} & \vdots & d_{n_s,n_c} \end{pmatrix} \cdot \begin{pmatrix} e_{1,1} & \cdots & e_{1,n_w} \\ \vdots & \ddots & \vdots \\ e_{n_c,1} & \cdots & e_{n_c,n_w} \end{pmatrix}. \end{aligned} \quad (2)$$

Here n_s denotes the number of different spectra (samples), each measured at n_w discrete wavelengths. Both n_w and n_s should be greater than n_c and we suppose for simplicity that $n_w > n_s$, since this is the common case.

Example PY + β -CD: Fig. 1 shows the series of spectra which form \mathbf{Y} with $n_w = 150$ and $n_s = 22$.

If the component spectra \mathbf{E} were known, \mathbf{D} could be determined by linear regressions, $\mathbf{D} = \mathbf{Y} \cdot \mathbf{E}^+$, and vice versa. But in many cases, neither \mathbf{E} nor \mathbf{D} and not even the number of contributing species n_c are known and estimates have to be found for all of them.

Can we determine the number of component spectra n_c without knowing the component spectra \mathbf{e}_j themselves?

Yes, taking into account that the experimental spectra \mathbf{Y} are linear combinations of the n_c distinct (linearly independent) component spectra \mathbf{e}_j (plus noise). The spectra \mathbf{e}_j span a space of *dimension* n_c and each of the experimental spectra \mathbf{y}_i is defined by a specific set of contributions d_{ij} which represent “coordinates” within this n_c -dimensional space. In matrix terms, we can say that $\text{rank}(\hat{\mathbf{Y}}) = n_c$. Thus, the minimal number of (any) linearly independent spectra needed to reproduce the systematic variation in the series of experimental spectra gives directly the number of observable components n_c . As we do not know the component spectra \mathbf{E} themselves, we express \mathbf{Y} by some other “abstract” spectra \mathbf{V} with coefficients \mathbf{Z} :

$$\mathbf{y}_i = z_{i1}\mathbf{v}_1 + z_{i2}\mathbf{v}_2 + \cdots + z_{in_s}\mathbf{v}_{n_s}. \quad (3)$$

In PCA, the vectors \mathbf{v}_i are the (left) *eigenvectors* of the quadratic and symmetric matrix $\mathbf{Y}^T\mathbf{Y}$, which has the same rank as \mathbf{Y} . The *eigenvectors* \mathbf{v}_i are solutions of the eigenvalue equation (4) and are easily computed, for example, in Matlab (The MathWorks, MA, USA) with one line of code: `[V, L] = eig(Y'Y); V = V';`

$$\underset{n_s \times n_w}{\mathbf{V}} \underset{n_w \times n_w}{\mathbf{Y}^T\mathbf{Y}} = \underset{n_s \times n_s}{\Lambda} \underset{n_s \times n_w}{\mathbf{V}}. \quad (4)$$

The eigenvectors \mathbf{V} reproduce all the variation in the experimental data \mathbf{Y} , including the noise.

$$\underset{n_s \times n_w}{\mathbf{Y}} = \underset{n_s \times n_s}{\mathbf{Z}} \cdot \underset{n_s \times n_w}{\mathbf{V}}. \quad (5)$$

The product $(z_{il} \mathbf{v}_l)$ defines the l th *principal component* (PC) of the i th experimental spectrum \mathbf{y}_i (see (3)).

The eigenvectors \mathbf{v}_l are orthogonal, that is $\mathbf{V}^T = \mathbf{V}^{-1}$, so that the matrix of coefficients \mathbf{Z} is easily calculated:

$$\mathbf{Z} = \mathbf{Y} \cdot \mathbf{V}^{-1} = \mathbf{Y} \cdot \mathbf{V}^T. \quad (6)$$

The diagonal matrix $\mathbf{\Lambda}$ contains the eigenvalues λ_l , sorted so that the first has the highest value. The eigenvalues indicate directly how much of the *total* variance $\text{SS}(\mathbf{Y}) = \sum_{i=1}^{n_s} \sum_{j=1}^{n_w} y_{ij}^2 = \sum_{l=1}^{n_s} \lambda_l$ in \mathbf{Y} is contributed by the l th PC:

$$\lambda_l = \sum_{i=1}^{n_s} \sum_{j=1}^{n_w} (z_{il} \mathbf{v}_{lj})^2 = \sum_{i=1}^{n_s} z_{il}^2. \quad (7)$$

In the absence of noise in \mathbf{Y} , the first n_c eigenvectors would reproduce all the variation in \mathbf{Y} . The eigenvalues corresponding to the remaining $(n_s - n_c)$ eigenvectors would be zero. In practice, however, each of the n_s experimental spectra will have a unique, linearly independent noise pattern, and for a full reproduction of \mathbf{Y} , n_s eigenvectors are needed, and in general $\text{rank}(\mathbf{Y}) = n_s > n_c$. Nevertheless, n_c can be estimated by making the following assumption: The systematic (correlated) variation in the spectra due to n_c chemical components forms the main part of the total variation in \mathbf{Y} , clearly separated from the (uncorrelated) variation due to noise or measurement imperfections. Thus, this “structural” variance is assumed to be reproduced by the first n_c PCs with the highest eigenvalues, whereas the remaining PCs represent the “residual” variance due to noise. The first n_c structural PCs will be represented by the truncated matrices $\tilde{\mathbf{V}}(n_c \times n_w)$, $\tilde{\mathbf{Z}}(n_s \times n_c)$, and $\tilde{\mathbf{\Lambda}}(n_c \times n_c)$. A superscript k at these matrices (e.g., $\tilde{\mathbf{V}}^k$) indicates that they are further cut down to only the first k PCs. The two sets of spectra \mathbf{E} and \mathbf{V} are then related by a “rotation” matrix \mathbf{P}

$$\underset{n_c \times n_w}{\mathbf{E}} = \underset{n_c \times n_c}{\mathbf{P}} \cdot \underset{n_c \times n_w}{\tilde{\mathbf{V}}} \quad \underset{n_s \times n_c}{\tilde{\mathbf{Z}}} = \underset{n_s \times n_c}{\mathbf{D}} \cdot \underset{n_c \times n_c}{\mathbf{P}}. \quad (8)$$

The following plots are used in order to discriminate between structural and residual PCs:

Eigenvector diagrams: Eigenvectors \mathbf{V} and (normalized) coefficients $\mathbf{Z}^* = \mathbf{\Lambda}^{-1/2} \mathbf{Z}^T$, which represent structural variation, can in general be well distinguished from those eigenvectors reproducing mainly noise or measurement imperfections and which change randomly with the variable.

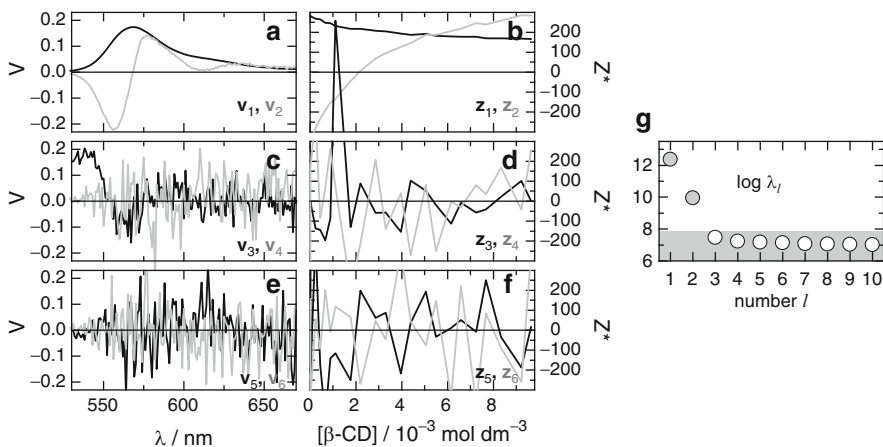


Fig. 2 Eigenvectors \mathbf{V} , (normalized) coefficients $\mathbf{Z}^* = \mathbf{\Lambda}^{-1/2}\mathbf{Z}$, and eigenvalues of the emission spectra \mathbf{Y} of the system PY + β -CD ($n_c = 2$) given in Fig. 1. (a, b) The structural components $\mathbf{v}_1, \mathbf{z}_1$ and $\mathbf{v}_2, \mathbf{z}_2$; (c)–(f) four residual components $\mathbf{v}_3, \mathbf{z}_3$ to $\mathbf{v}_6, \mathbf{z}_6$. Higher components are similar and not shown. (g) The first ten eigenvalues λ_1 – λ_{10} . The first two eigenvalues (gray) belong to structural components, the other to residual components

Example PY + β -CD: The first two eigenvectors \mathbf{v}_1 and \mathbf{v}_2 shown in Fig. 2 vary systematically with wavelength. Comparing \mathbf{v}_1 with the spectra in Fig. 1, it is easily seen that it represents a mean spectrum reproducing the overall shape of the spectra. Its coefficient \mathbf{z}_1 drops with increasing host concentration following the decrease in overall emission. The second eigenvector \mathbf{v}_2 has just the form necessary to introduce the displacement of the spectrum to longer wavelength as its coefficient \mathbf{z}_1 increases from negative to positive values. These two first PCs reproduce already 96.4% of the total variance, the rest being mostly due to noise, as can be deduced from the uncorrelated variation of the following eigenvectors and coefficients $\mathbf{v}_3, \mathbf{z}_3$ to $\mathbf{v}_6, \mathbf{z}_6$.

Log-Eigenvalue Diagram: In the logarithmic plot of the eigenvalues λ_l vs. l , the residual eigenvalues define the level of “noise” variance. The number of PCs with an eigenvalue above this level give an upper limit for the number of structural components.

Example PY + β -CD: The first two of the eigenvalues shown in Fig. 2 are much higher than the following ones and represent the structural variance in the data reproduced by the first two PCs.

Residual Spectra: In order to detect systematic variation in \mathbf{Y} not reproduced by the first k components, one can inspect residuals \mathbf{R}^k between the experimental spectra \mathbf{Y} and estimated spectra $\hat{\mathbf{Y}}^k$, which are calculated by including only the first k PCs. Residuals calculated with less than n_c PCs ($k < n_c$) show systematic deviations.

$$\mathbf{R}^k = \mathbf{Y} - \hat{\mathbf{Y}}^k = \mathbf{Y} - \tilde{\mathbf{Z}}^k \tilde{\mathbf{V}}^k. \quad (9)$$

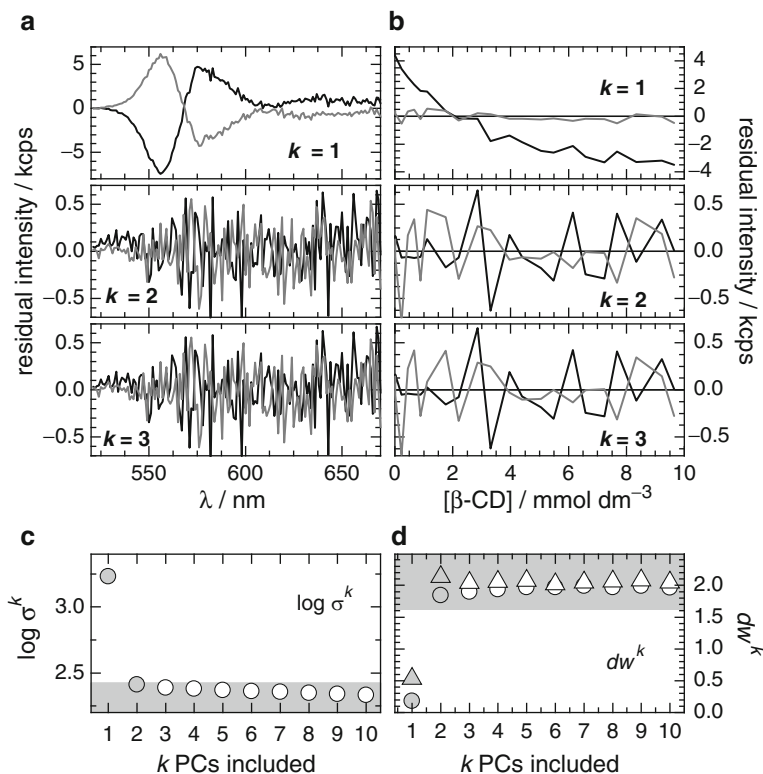


Fig. 3 Determination of the number of structural components from PCA of the emission spectra of Fig. 1. (a) Residual spectra R^k at two concentrations of β -CD: 0 mM (black) and 9.7 mM (gray) for $k = 1, 2$, and 3. (b) Residual profiles $(R^k)^T$ at two wavelengths 580 nm (black) and 610 nm (gray) for $k = 1, 2$, and 3. (c) Mean residual error σ^k vs. the number of included PCs k . (d) Mean Durbin-Watson Test values dw^k of residual spectra r_{ij} (circles) and of residual profiles r_{ji} (triangles) vs. the number of included PCs k . Values within the gray shaded area indicate uncorrelated residuals

The representation of these residual spectra r_{ij}^k vs. wavelength index j with successively increasing number of components k yields important information, revealing at which wavelengths and at which values of the external variable systematic deviations can be observed. Although variations in the PCs have no direct physical significance, typical influences of Raman bands, change-over wavelength of light sources, or strong baseline instabilities may be identified readily and be taken into account.

Example PY + β -CD: The residual spectra (Fig. 3) show random variation after inclusion of two components ($k = 2$).

Mean Residual Error Diagram: The mean residual error σ^k is estimated from the weighted root mean square of the residuals r_{ij}^k (9). Once all structural PCs are included, that is for $k \geq n_c$, the mean residual error reaches some constant level of instrumental noise.

$$\sigma^k = \left(\frac{\sum_{i=1}^{n_s} \sum_{j=1}^{n_w} (y_{ij} - \hat{y}_{ij}^k)^2}{(n_s - k)(n_w - k)} \right)^{1/2} = \left(\frac{\sum_{l=k+1}^{n_s} \lambda_l}{(n_s - k)(n_w - k)} \right)^{1/2}. \quad (10)$$

Example PY + β -CD: The inclusion of two components reduces the value of the mean residual error down to the noise level (Fig. 3c).

Durbin–Watson Test of the Residuals: The plot of mean Durbin–Watson Test values dw^k measures the correlation between consecutive values of the residuals r_{ij}^k . The residuals become uncorrelated for $k \geq n_c$. Uncorrelated residuals are indicated by the values of $dw^k > 1.5$ – 1.7 depending on n_w . [7, 8].

$$dw_i^k = \frac{\sum_{j=2}^{n_w} (r_{i,j}^k - r_{i,j-1}^k)^2}{\sum_{j=1}^{n_w} (r_{i,j}^k)^2}. \quad (11)$$

Example PY + β -CD: The mean Durbin–Watson Test values of the residual spectra (black circles in Fig. 3d) exceed the critical value of about 1.7 with the inclusion of the second component.

Residual Profiles: Series of experimental absorption or emission spectra are subject not only to random noise but also to erroneous variations of instrumental and experimental conditions such as baseline, detector sensitivity, source lamp intensity, or background counts. These may introduce systematic spectral variations which will appear in PCA as “spurious” components which are not easily distinguishable from structural components corresponding to chemical species. Structural and spurious components can be differentiated by analyzing the variation in the residuals as a function of the external variable, representing the *residual profiles* $(\mathbf{R}^k)^T$. The contribution of the spurious components most probably does not follow in any systematic way the change in the external variable and should lead to random variation in the residual profiles. This can also be detected effectively in the Durbin–Watson Test values of the residual profiles.

Example PY + β -CD: In this system, the residual profiles show uncorrelated noise with two or more included PCs which is confirmed by their mean Durbin–Watson Test values (Fig. 3b and white circles in Fig. 3d). An example of spurious components can be seen in the case of HBI in Sect. 5.2. We conclude here that PCA of the emission spectra of PY in the presence of β -CD indicate that only two components are necessary to explain the observed systematic variation.

4 Model Validation and Parameter Estimation by Global Analysis

Nonlinear regression is a well established and widely applied technique for the estimation of model parameters. The simultaneous analysis of multiple series of experimental data sharing common model parameters, known as global analysis

(GA), had been introduced for fluorescence lifetime and anisotropy analysis [3, 6, 13, 27] and is extensively used in many areas of physical chemistry. Both specialized and general purpose programs for global nonlinear analysis can be found. Nevertheless, the great benefit of global analysis not only for parameter estimation but also for the much more valuable testing and validation of models is still strongly underestimated and has not been established as a standard tool in many laboratories. We will give in the following a short introduction to the theory of global nonlinear analysis of series of spectra and apply it to the example systems.

The basic procedure is straightforward. It comprises three steps: (a) postulation of a model defining the matrix of contributions (concentrations) \mathbf{D} as a function of parameters and of the external variable; (b) estimation of the parameters in \mathbf{D} and of the values of the component spectra \mathbf{E} by iterative nonlinear least-squares fit of $\hat{\mathbf{Y}} = \mathbf{D} \cdot \mathbf{E}$ to the experimental data matrix \mathbf{Y} ; and (c) test of the adequacy of the used model on the basis of the goodness of the fit.

The elements of the matrix of contributions d_{il} are n_c (nonlinear) model functions h_l of the external variable x_i (pH, initial concentrations of some reactant, time, etc.) and depends on model parameters a, b, \dots such as equilibrium or rate constants:

$$\hat{d}_{il} = h_l(a, b, \dots; x_i), \quad i = 1 \dots n_s, \quad l = 1 \dots n_c. \quad (12)$$

Nonlinear minimization then applies some iterative algorithm such as that of Marquardt [4, 21] in order to find values of the a, b, \dots and $\hat{\mathbf{E}}$ which minimize the sum of squares of the residuals χ^2 between \mathbf{Y} and $\hat{\mathbf{D}}\hat{\mathbf{E}}$:

$$\chi^2 = \sum_{i=1}^{n_s} \sum_{j=1}^{n_w} \left((\mathbf{Y} - \hat{\mathbf{D}}\hat{\mathbf{E}})_{ij} \right)^2 = \sum_{i=1}^{n_s} \sum_{j=1}^{n_w} \left((\mathbf{Y} - \hat{\mathbf{D}}(\hat{\mathbf{D}}^+ \mathbf{Y}))_{ij} \right)^2. \quad (13)$$

In this procedure, the model parameters a, b, \dots are estimated by iterative nonlinear minimization, whereas the $(n_c \cdot n_w)$ linear component spectra in $\hat{\mathbf{E}}$ are determined in each iteration directly by linear regression $\hat{\mathbf{E}} = \hat{\mathbf{D}}^+ \mathbf{Y}$, that is by multiplying \mathbf{Y} with the pseudo inverse of $\hat{\mathbf{D}}$ calculated with the given values of a, b, \dots in each iteration [14]. This way the number of unknown (linear) parameters is tremendously reduced.

In the case of a very big experimental matrix \mathbf{Y} , it can be useful to reduce the size of the matrices from $(n_s \times n_w)$ to $(n_s \times n_c)$ using the information from PCA: $\hat{\mathbf{Y}} = \tilde{\mathbf{Z}}\tilde{\mathbf{V}}$ (5) and $\hat{\mathbf{E}} = \tilde{\mathbf{P}}\tilde{\mathbf{V}}$ (8). The small rotation matrix $\tilde{\mathbf{P}}$ can again be estimated by linear regression $\tilde{\mathbf{P}} = \hat{\mathbf{D}}^+ \tilde{\mathbf{Z}}$.

$$\chi^2 = \sum_{i=1}^{n_s} \sum_{j=1}^{n_w} \left((\tilde{\mathbf{Z}}\tilde{\mathbf{V}} - \hat{\mathbf{D}}\tilde{\mathbf{P}}\tilde{\mathbf{V}})_{ij} \right)^2 = \sum_{i=1}^{n_s} \sum_{l=1}^{n_c} \left((\tilde{\mathbf{Z}} - \hat{\mathbf{D}}(\hat{\mathbf{D}}^+ \tilde{\mathbf{Z}}))_{il} \right)^2. \quad (14)$$

The values of the parameters a, b, \dots and the component spectra $\hat{\mathbf{E}}$ are the result of the global analysis of all the $(n_s \times n_w)$ measurements available in the

experiment. This has several important consequences: (1) The much higher number of data points leads in general to much smaller statistical errors in the parameters as compared to the standard analysis at one (or few) wavelength with only $(n_s \times 1)$ data points. (2) Correlations between the parameters e_{ij} , a , b , ... are reduced [11]. (3) A model and a set of parameter values which may be valid at a single wavelength or in some small wavelength range may fail to reproduce the data at the full wavelength interval. Checking a model against the full spectra is a much more demanding test and gives much more confidence in the validity of the model than single wavelength fits. (4) The component spectra obtained from this analysis constitute themselves an important result, since usually some of them cannot be determined directly.

Example PY + β -CD: From PCA, we know now that two components are responsible for the variation of the emission spectra of the PY with β -CD. If a 1:1 complexation equilibrium in the ground state is proposed, the two components are identified as free pyronine (\mathbf{e}_1) and its complex with β -CD (\mathbf{e}_2). Under the conditions of constant PY concentration and excess of β -CD, the following equations describe the relative concentrations of free pyronine (d_{i1}) and its complex (d_{i2}) as a function of the β -CD concentration and the association equilibrium constant K :

$$\hat{d}_{i1} = \frac{1}{1 + K[CD]_i}, \quad \hat{d}_{i2} = \frac{K[CD]_i}{1 + K[CD]_i}. \quad (15)$$

The results of the fit of (15) to the emission spectra of Fig. 1 are given in Table 1. The individual fits at three wavelengths give three values of K which span a wide interval with huge uncertainties. The global analysis at the same three wavelengths yields a common value of K with smaller uncertainty which assures a consistent fit at the three wavelengths. Finally, fitting all wavelengths simultaneously following (13), not only the smallest uncertainty in K is obtained but also the whole component spectra \mathbf{e}_j as shown in Fig. 4. The spectrum of the free dye PY is known and coincides perfectly with \mathbf{e}_1 , but that of the complex PY: β -CD, \mathbf{e}_2 , cannot be measured directly, since it is not possible to get a concentration of β -CD high enough to have all the PY complexed.

Table 1 Results of nonlinear regression of (15) to the emission spectra of Fig. 1

λ/nm	Individual analysis			Global analysis		
	K/M^{-1}	$e_1/10^4$	$e_2/10^4$	K/M^{-1}	$e_1/10^4$	$e_2/10^4$
555	372 ± 18	5.7 ± 0.3	1.5 ± 0.6		5.7 ± 0.4	1.5 ± 0.6
565	411 ± 35	7.6 ± 0.6	3.3 ± 1.0	399 ± 19	7.6 ± 0.4	3.2 ± 0.7
575	438 ± 61	6.5 ± 0.5	4.0 ± 0.9		6.5 ± 0.4	4.0 ± 0.5
Global analysis (PCGA)						
$K = 397 \pm 4 \text{ M}^{-1}$						

Individual and global analyses at three wavelengths and global analysis (PCGA) at all wavelengths between 521 and 670 nm ($n_w = 150$). The values of the component spectra \mathbf{e}_j and the contributions \mathbf{d}_j from PCGA are shown in Fig. 4. The standard errors are determined from the variance-covariance matrix calculated as part of the nonlinear minimization [4, 22]

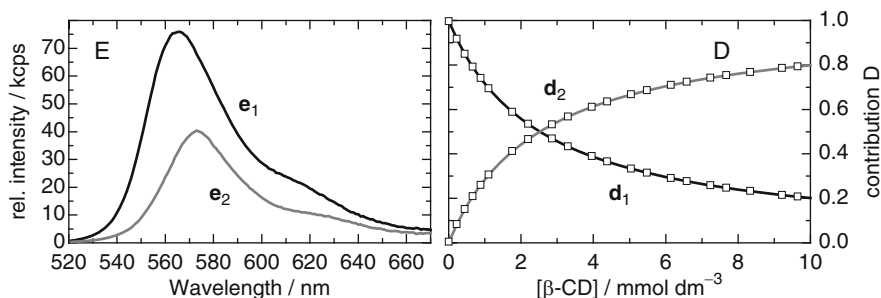


Fig. 4 Component spectra **E** and contributions **D** determined from PCGA of the emission spectra of the system PY + β -CD given in Fig. 1 and the value of K given in Table 1.

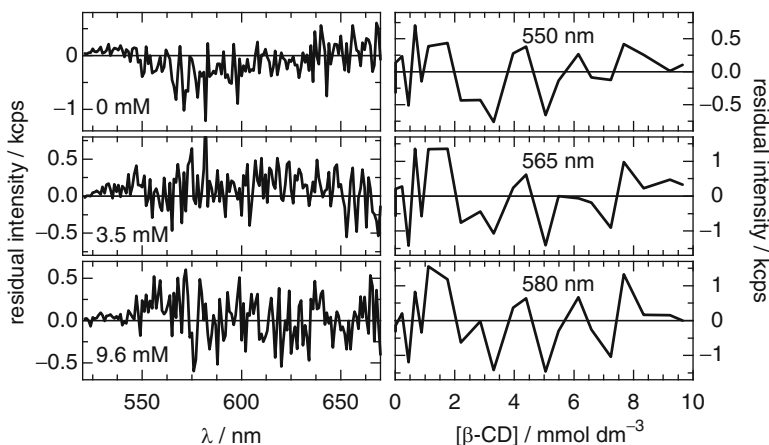


Fig. 5 Examples of the residuals $\mathbf{Y} - \hat{\mathbf{Y}}$ from the global analysis (PCGA) of the emission spectra \mathbf{Y} of Fig. 1. *Left column*: residual spectra ($\mathbf{Y} - \hat{\mathbf{Y}}$) at three concentrations of β -CD as given in the plots. *Right column*: residual profiles ($\mathbf{Y} - \hat{\mathbf{Y}})^T$ at three wavelengths as given in the plots

The goodness of the fits is checked on the basis of the residuals shown for certain wavelengths and host concentrations in Fig. 5. The randomly distributed residuals indicate good fits and validate the proposed model.

5 Results for the Example Systems

Here, we apply PCGA to some typical physicochemical systems. The results for the host–guest interaction between PY and CD have already been used to illustrate the method. The first example (Sect. 5.1) is that of a host–guest association with 1:1 and 1:2 host:guest stoichiometry and thus with three components. The following system (Sect. 5.2) shows two acid–base equilibria in the ground and the excited states and

the third system (Sect. 5.3) a complex dependence of the concentration of different species coupled by excited-state proton-transfer reactions.

5.1 Host–Guest Association Equilibria Between TNS and a Charged Cyclodextrin Derivative

The complexation of 2-(*p*-toluidinyl)naphthalene-6-sulfonate (TNS) with the positively charged cyclodextrin, 6-deoxy-6-amino- β -cyclodextrin (CD) involves the simultaneous formation of two different 1:1 complexes, resulting from inclusion of the toluidin moiety or the naphthalenesulfonate moiety in a cyclodextrin unit, and a 1:2 complex, which is due to the complexation of the two aromatic moieties of TNS with two cyclodextrin molecules. The resolution of this complicated system, with four emitting species and four association equilibria, could only be achieved by careful and systematic analysis of both steady-state and time-resolved fluorescence data, together with direct structural information from NMR experiments [2].

Figure 6 shows the emission spectra ($n_s = 13$) of TNS at varying CD concentrations. PCA of these spectra indicates in all cases clearly three structural components as can be observed in Fig. 7. While the first three eigenvectors \mathbf{v}_1 – \mathbf{v}_3 vary systematically with wavelength, the fourth eigenvector \mathbf{v}_4 shows already variations which are of the order of the noise itself and is not different from the following eigenvectors \mathbf{v}_5 or \mathbf{v}_6 . The same is true for the coefficient \mathbf{z}_1 – \mathbf{z}_6 and is confirmed by the plots of the eigenvalues λ_i , the mean residual error σ^k , and the Durbin–Watson Test values dw^k .

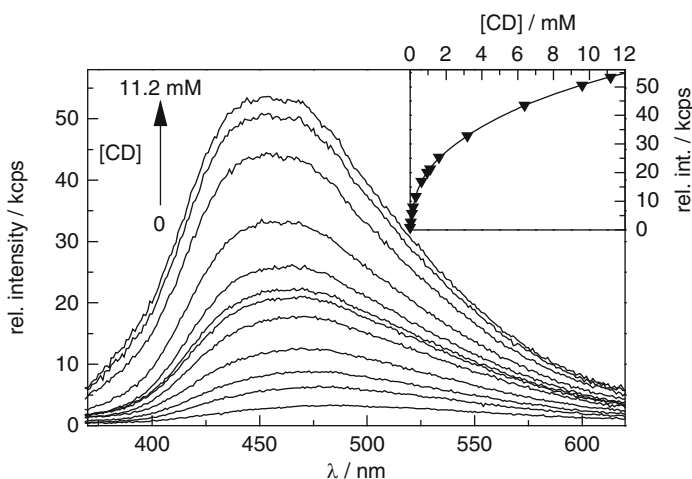


Fig. 6 Corrected fluorescence emission spectra ($\lambda_{\text{exc}} = 320 \text{ nm}$) of TNS in the presence of different concentrations of CD in the range from 0 to $11.2 \times 10^{-3} \text{ M}$. $[\text{TNS}] = 2.0 \times 10^{-6} \text{ M}$. *Inset*: Fluorescence intensity at 450 nm vs. CD concentration

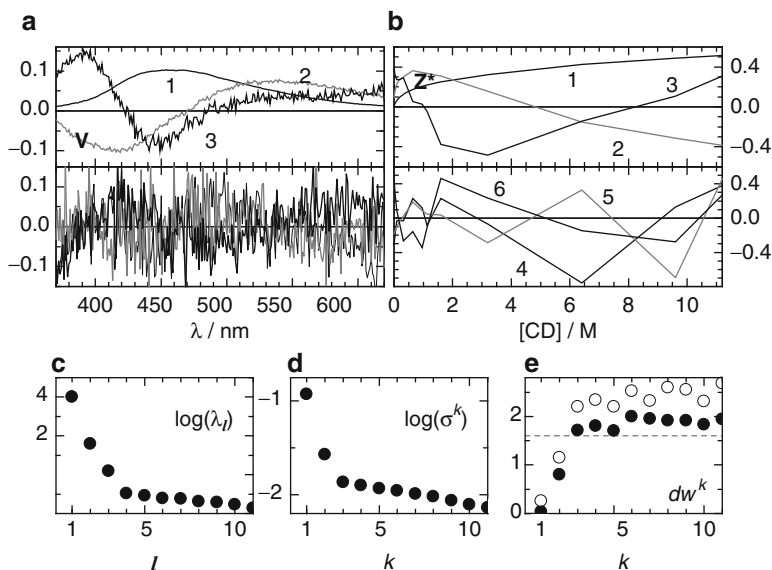
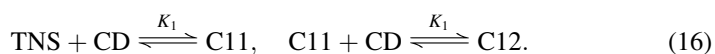


Fig. 7 Determination of the number of structural components n_c from PCA of the emission spectra of TNS (Fig. 6). (a) Eigenvectors \mathbf{v}_1 – \mathbf{v}_3 (above) and \mathbf{v}_4 – \mathbf{v}_6 (below). (b) (Normalized) coefficients $\mathbf{Z}^* = \Lambda^{-1/2}\mathbf{Z}$, \mathbf{z}_1 – \mathbf{z}_3 (above) and \mathbf{z}_4 – \mathbf{z}_6 (below). (c) Eigenvalues λ_1 – λ_{11} . (d) Mean residual error σ^k vs. the number of included PCs k . (e) Mean Durbin–Watson Test values dw^k of residual spectra r_{ij} (black circles) and of residual profiles r_{ji} (open circles) vs. the number of included PCs k

In order to account for the three structural components found by PCA, the components are assigned to the chemical species, free TNS, 1:1 complex (C11) and 1:2 complex (C12), and a mechanism with two complexation equilibria was proposed:



This model does not take into account that two different 1:1 complexes are formed, since their concentrations have the same dependence on CD concentration. Their existence cannot be derived from steady-state fluorescence measurements, but from time-resolved fluorescence studies.

In the absence of interconversion processes in the excited state and under conditions of excess CD concentration ($[\text{CD}] \approx [\text{CD}]_0$), the following equations for the concentrations \mathbf{D} of the three species, TNS, C11, and C12, are obtained.

$$\begin{pmatrix} \hat{d}_{11} & \hat{d}_{12} & \hat{d}_{13} \end{pmatrix} = \begin{pmatrix} a & a \cdot K_1[\text{CD}] & a \cdot K_1 K_2[\text{CD}]^2 \end{pmatrix} \\ \text{with } a = (1 + K_1[\text{CD}] + K_1 K_2[\text{CD}]^2)^{-1}. \quad (17)$$

The fit of (17) to single emission intensity profiles as a function of $[\text{CD}]$ allows for the determination of the association constants K_1 and K_2 . Nevertheless, strong

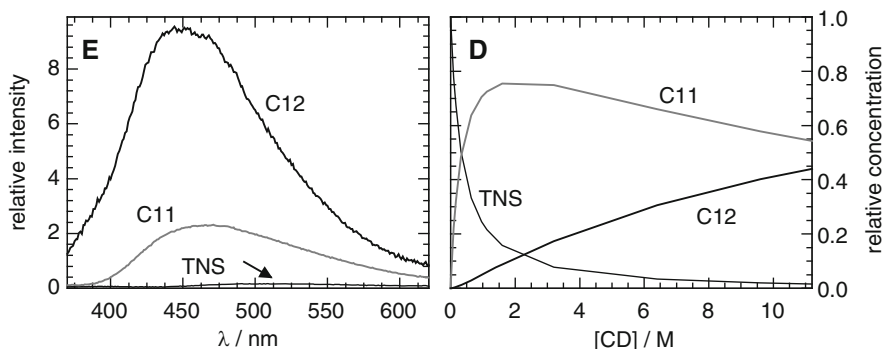


Fig. 8 Results of PCGA of the emission spectra of TNS (Fig. 6). *Left*: component spectra **E** corresponding to free TNS, 1:1 complex (C11), and 1:2 complex (C12). *Right*: coefficients **D** representing the relative concentrations of the species TNS, C11, and C12 ($K_1 = (2.99 \pm 0.03) \times 10^3 \text{ M}^{-1}$, $K_2 = 72 \pm 1 \text{ M}^{-1}$)

correlation is observed between the nonlinear parameter K_2 and the linear parameter e_{3j} , since only a small percentage of the complex C12 is present even at the highest [CD]. This correlation is efficiently reduced in the global analysis and precise values for the equilibrium constants and for the component spectra are obtained (Fig. 8). Note that the emission spectrum of complex C11 is a combination of the spectra of the two 1:1 complexes present. As these two species show the same dependence on [CD], they appear as an only component in PCA.

5.2 Excited-State Proton Transfer of 2-(2'-Hydroxyphenyl) Benzimidazole

In aqueous solutions, 2-(2'-hydroxyphenyl)benzimidazole (HBI) shows in the ground state two acid–base equilibria and a tautomeric equilibrium of three neutral species (Fig. 9). In the excited state, several photoinduced proton-transfer reactions were detected [1, 18]. The cationic form C^* deprotonates very fast at the hydroxyl group, only emission from the keto form K^* being detected at acidic pH. The neutral *cis*-enol form E_c^* experiments an excited-state intramolecular proton transfer, leading also very fast to the neutral keto form K^* . The *trans*-enol form E_t^* also deprotonates at the hydroxyl group, leading to the excited anion A^* , but some fluorescence from E_t^* is also detected. The emission spectra of HBI in aqueous solutions change significantly with pH and show strong spectral overlap (Fig. 10).

The results of PCA of the emission series of HBI (Fig. 10) are shown in Fig. 11. All plots reveal the presence of three structural components. The variance of the fourth component (see λ_4) is still slightly higher than that of the following residual components. This additional variance is due to some systematic variation in the residual spectra (see v_4 and residual spectra with $k = 3$) but not in the dependence

Fig. 9 Acid–base, tautomeric and conformational equilibria of HBI in aqueous solution. Molecular structures of HBI: **C** cationic form, **K** keto form, **E_t** *trans*-enol form, **E_c** *cis*-enol form, and **A** anionic form. Fluorescent species are set in **bold** letters

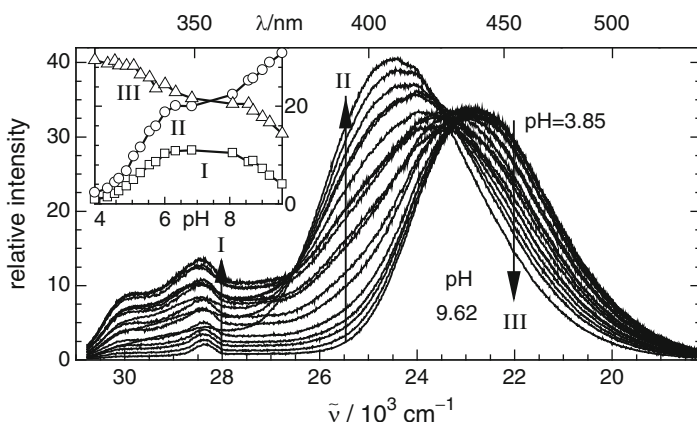
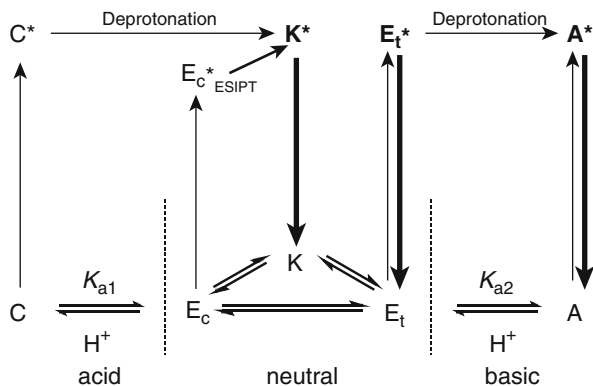


Fig. 10 Series of fluorescence emission spectra of HBI in aqueous solution with varying pH values between 3.85 and 9.62. $[HBI] = 2.4 \times 10^{-6} \text{ M}$, $\tilde{\nu}_{exc} = 31,650 \text{ cm}^{-1}$. The count rates have been divided by 10^6 cps. Peaks at $28,350 \text{ cm}^{-1}$ are due to Raman scattering. *Inset*: emission intensity profiles at the indicated wavenumbers

on pH (see **z₄** and residual profiles with $k = 3$). This is a typical pattern found for “spurious” components introduced by instrumental or experimental error during the measurement which does not depend on the external variable. We therefore confirm that three structural components are present, which according to the mechanism described above are assigned to the excited anion **A*** and the neutral keto **K*** and *trans*-enol **E_t*** forms.

On the basis of the mechanism described, model functions for the component contributions d_{ij} are proposed in (18), which were globally fitted to the series of spectra as a function of pH. d_{i1} represents the pH dependence of the anion emission, with contributing terms from the excitation of the ground-state anion and from the photoinduced emission of the anion at neutral pH, formed from the excited

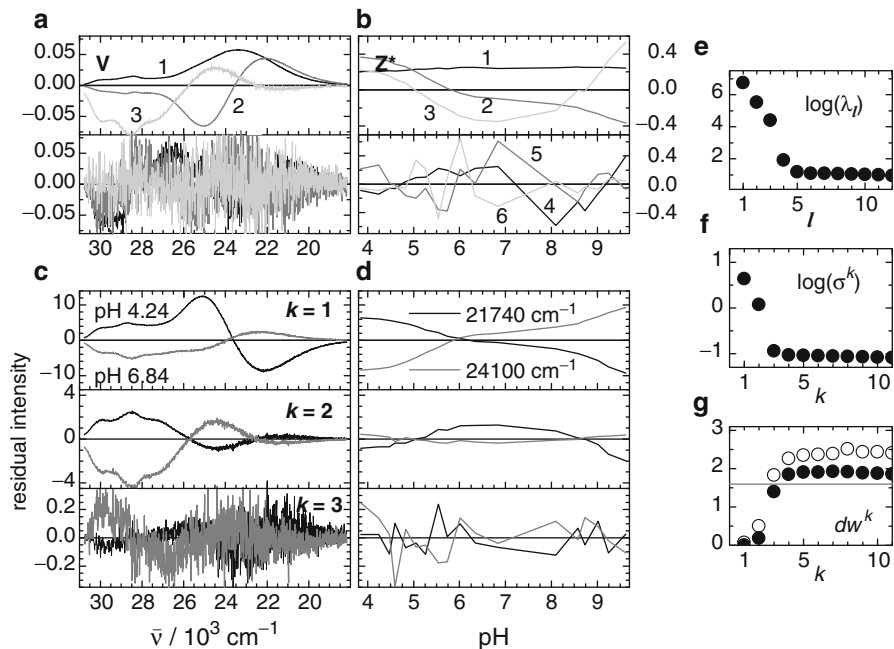


Fig. 11 PCA of the emission spectra of HBI (Fig. 10). (a) Eigenvectors \mathbf{v}_1 – \mathbf{v}_3 (above) and \mathbf{v}_4 – \mathbf{v}_6 (below). (b) (Normalized) coefficients $\mathbf{Z}^* = \mathbf{\Lambda}^{-1/2}\mathbf{Z}$, \mathbf{z}_1 – \mathbf{z}_3 (above), and \mathbf{z}_4 – \mathbf{z}_6 (below). (c) Residual spectra \mathbf{R}^k at two pH: 4.24 (black) and 6.84 (gray) for $k = 1, 2$, and 3 included PCs. (d) Residual profiles $(\mathbf{R}^k)^T$ at $21,740 \text{ cm}^{-1}$ (black) and $24,100 \text{ cm}^{-1}$ (gray) for $k = 1, 2$, and 3 . (e) Eigenvalues λ_1 – λ_{10} . (f) Mean residual error σ^k vs. the number of included PCs k . (g) Mean Durbin–Watson Test values dw^k of residual spectra r_{ij} (black circles) and of residual profiles r_{ji} (open circles) vs. the number of included PCs k

trans-enol form. d_{i2} represents the pH dependence of the *trans*-enol form emission. d_{i3} represents the pH dependence of the keto form emission, with contributing terms from the photoinduced formation of \mathbf{K}^* by deprotonation of the excited cation at acidic pH, and from the excitation of the neutral forms \mathbf{E}_c and \mathbf{K} . The values of γ and β have been obtained from comparison of excitation and absorption spectra and maintained constant in the fit. The resulting pK_a values, pure component spectra, and component contributions are given in Fig. 12.

$$\begin{aligned}
 (\hat{d}_{i1} \quad \hat{d}_{i2} \quad \hat{d}_{i3}) &= (a(K_{a1}K_{a2} + \gamma K_{a1}[\text{H}^+]_i) \quad aK_{a1}[\text{H}^+]_i \quad a([\text{H}^+]_i^2 + \beta K_{a1}[\text{H}^+]_i)) \\
 &\quad \text{with } a = (K_{a1}K_{a2} + K_{a1}[\text{H}^+]_i + [\text{H}^+]_i^2)^{-1}.
 \end{aligned} \quad (18)$$

5.3 Lactim–Lactam Phototautomerization

Ground-state tautomeric and acid–base equilibria, and excited-state proton-transfer processes of 2-(6'-hydroxy-2'-pyridyl)benzimidazole (HPyBI) in aqueous solution

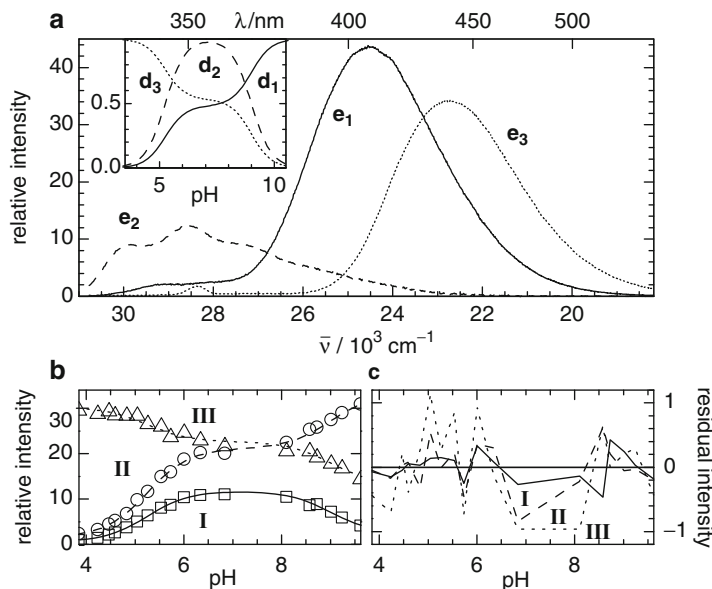


Fig. 12 Results of the global analysis of the emission spectra of HBI (Fig. 10) according to (18) and parameters $pK_{a1} = 5.246 \pm 0.002$ and $pK_{a2} = 8.996 \pm 0.004$, and fixed parameters $\beta = 0.53$ and $\gamma = 0.48$ obtained from excitation and absorption spectra. (a) Resolved component spectra e_1 (solid), e_2 (dashed), and e_3 (dotted) corresponding to the species A^* , E_t^* , and K^* , respectively. The peaks at $28,350 \text{ cm}^{-1}$ are due to Raman scattering. *Inset*: Relative concentrations D vs. pH. (b) pH dependence of the experimental Y (symbols) and fitted \hat{Y} (lines) fluorescence intensity at three spectral positions as indicated in Fig. 10. (c) Residual intensity profiles between the Y and \hat{Y} of (b)

have been studied by means of UV–vis absorption and fluorescence spectroscopy in both steady-state and time-resolved modes [19, 20]. There exist a lactim–lactam tautomeric equilibrium for both the neutral (N and T) and the protonated forms (C and TC) in the ground state (Fig. 13). An acid–base equilibrium between the protonated and neutral forms is established, with $pK_a = 3.127$. The excited-state behavior is summarized in Fig. 13. The increase of acidity of the OH group and basicity of the pyridine nitrogen upon excitation originates the phototautomerization of the neutral N and protonated C lactim species upon excitation. For the protonated form (Fig. 13b), the lactim–lactam phototautomerization process takes place via two competitive excited-state proton-transfer routes: a one-step water-assisted proton translocation (probably a double proton transfer) and a two-step pathway which involves first the dissociation of the lactim cation to form an emissive intermediate zwitterionic species and then the acid-catalyzed protonation at the pyridine nitrogen to give rise to the lactam tautomer. For the neutral lactim form, only the first route has been detected (Fig. 13a).

PCA was applied to the series of 28 fluorescence spectra of HPyBI recorded in water under excitation at $31,250 \text{ cm}^{-1}$ (where only the lactim forms absorb) at different pH values (Fig. 14). The results of the analysis are shown in Fig. 15.

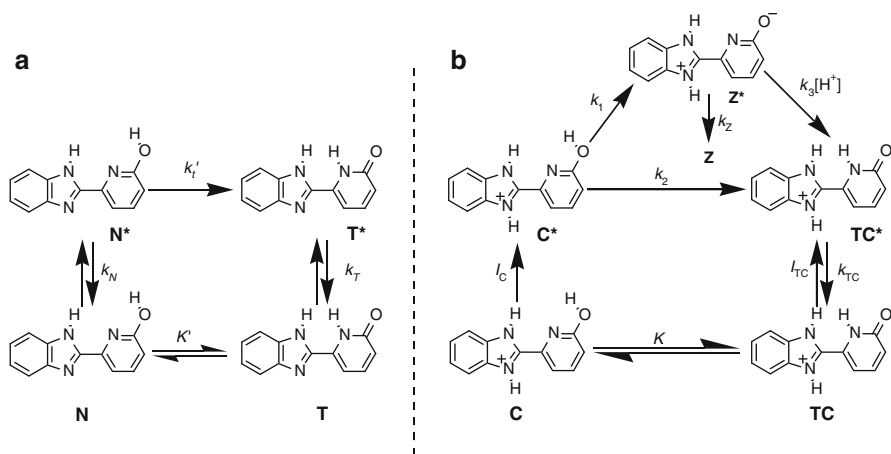


Fig. 13 Excitation and deactivation of (a) neutral and (b) protonated HPyBI in aqueous solution. The neutral (N and T) and protonated (C and TC) tautomeric forms are in equilibrium in the ground state, with $pK_a = 3.127$

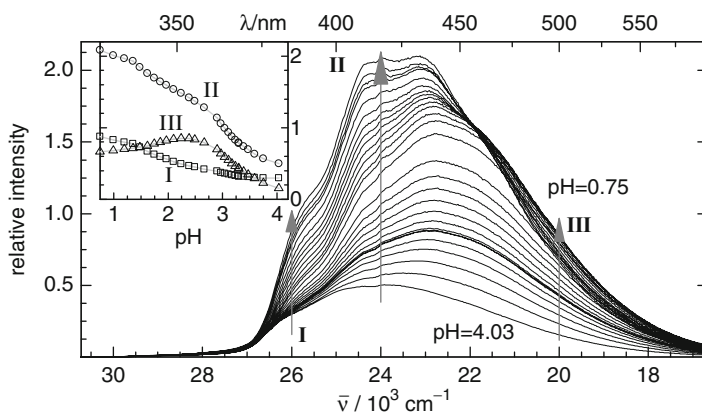


Fig. 14 Fluorescence spectra of HPyBI in aqueous solution with decreasing pH in the range 4.03–0.75. The inset shows the dependence on acidity of the fluorescence intensity at $\tilde{\nu}_{em} = 26,000 \text{ cm}^{-1}$ (open square), $24,010 \text{ cm}^{-1}$ (open circle), and at $20,000 \text{ cm}^{-1}$ (open triangle) ($n_s = 28$, $n_w = 550$, $\tilde{\nu}_{exc} = 31,250 \text{ cm}^{-1}$, $[\text{HPyBI}] = 3 \times 10^{-6} \text{ mol dm}^{-3}$)

The coefficients \mathbf{Z}^* , the eigenvalues λ , the mean residual error σ^k , and the mean Durbin–Watson Test dw^k of residual profiles demonstrate that three independent spectral components are needed to reproduce all the experimental spectra at the different acidities. The eigenvectors \mathbf{V} and the Durbin–Watson Test dw^k of the residual spectra (black circles in Fig. 15e) indicate some additional systematic spectral variation. The additional variance may be introduced by a very low

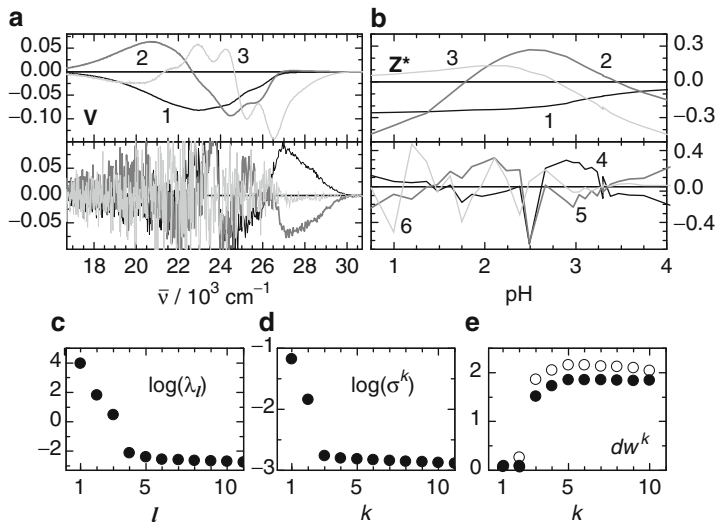


Fig. 15 Determination of the number of structural components n_c from PCA of the emission spectra of HPyBI (Fig. 14). (a) Eigenvectors \mathbf{v}_1 – \mathbf{v}_3 (above) and \mathbf{v}_4 – \mathbf{v}_6 (below). (b) (Normalized) coefficients $\mathbf{Z}^* = \mathbf{\Lambda}^{-1/2} \mathbf{Z}$, \mathbf{z}_1 – \mathbf{z}_3 (above) and \mathbf{z}_4 – \mathbf{z}_6 (below). (c) Eigenvalues λ_1 – λ_{11} . (d) Mean residual error σ^k vs. the number of included PCs k . (e) Mean Durbin–Watson Test values dw^k of residual spectra r_{ij} (black circles) and of residual profiles r_{ji} (open circles) vs. the number of included PCs k

emission from species \mathbf{C}^* , that is almost nonfluorescent because of the fast proton-transfer reactions in the excited state. The analysis shows that its fluorescence is almost undetectable.

Based on this information, a model with three components was proposed. In the working acidity range, the emissive species are \mathbf{N}^* , \mathbf{T}^* , \mathbf{Z}^* and \mathbf{TC}^* . As the acidity dependence of the steady-state concentrations of the neutral forms \mathbf{N}^* and \mathbf{T}^* is the same, both species will always be in a fixed proportion at the exciting wavenumber at any acidity and they will appear as one component \mathbf{NT}^* .

Taking into account the acidity dependence of the steady-state concentration of the respective excited species, the fluorescence emission spectra \mathbf{F} from the series can then be written as a linear combination of the spectra of the emissive species (The ratio $\beta = 0.468$ is known from time-resolved fluorescence results):

$$\mathbf{F} = c_{NT} \mathbf{F}_{NT} + c_2 ((1 - \beta) \mathbf{F}_Z + \beta \mathbf{F}_{TC}) + c_3 \mathbf{F}_{TC}. \quad (19)$$

The model functions for the concentrations have been derived from the proposed mechanism:

$$\begin{aligned} (c_{NT} \quad c_2 \quad c_3) &= \left(\frac{K_a}{K_a + [\text{H}^+]} \quad a[\text{H}^+] \quad a\alpha[\text{H}^+]^2 \right) \\ \text{with } a &= ((1 + \alpha[\text{H}^+])(K_a + [\text{H}^+]))^{-1}. \end{aligned} \quad (20)$$

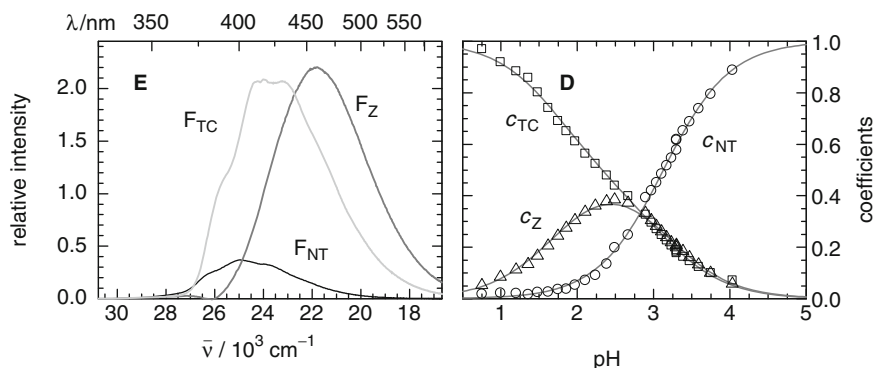


Fig. 16 Results of PCGA of the emission spectra of HPyBI (Fig. 14). *Left*: component spectra **E** corresponding to the neutral forms N^* and T^* (F_{NT}), the zwitterion Z^* (F_Z), and the lactam cation TC^* (F_{TC}). *Right*: coefficients **D** (unfilled symbols) representing the pH-dependent contributions of the component spectra of N^* and T^* (c_{NT}), Z^* (c_Z), and TC^* (c_{TC}). The solid lines represent the fit of the equations derived from the proposed model to these data. We used for these analyses the ratio $\beta = 0.468$ in H_2O provided from time-resolved fluorescence results

Global analysis with these model functions allowed us to obtain reliable estimations of the model parameters and the component spectra with $pK_a = 3.127 \pm 0.004$ and $\alpha = 57.3 \pm 1.2 \text{ mol dm}^{-3}$. This allows one to obtain the pure spectrum of Z^* and the coefficients c_{NT} , $c_Z = c_2(1 - \beta)$, and $c_{TC} = c_2\beta + c_3$ shown in Fig. 16. From the ratio of the areas beneath the species spectra, relative quantum efficiencies have been determined, which is especially interesting for the otherwise inaccessible zwitterion Z^* , which does not exist in the ground state [19].

Acknowledgments We thank the Spanish Ministry of Education and Science, the European Union ERDF, and the *Xunta de Galicia* for financial support.

References

1. Al-Soufi W, Novo M, Mosquera M (2001) Principal component global analysis of fluorescence and absorption spectra of 2-(2'-hydroxyphenyl)benzimidazole. *Appl Spectrosc* 55:630–636
2. Álvarez-Parrilla E, Al-Soufi W, Ramos Cabrer P, Novo M, Vázquez Tato J (2001) Resolution of the association equilibria of 2-(*p*-toluidinyl)-naphthalene-6-sulfonate (Tns) with beta-cyclodextrin and a charged derivative. *J Phys Chem B* 105:5994–6003
3. Beechem JM, Gratton E, Ameloot M, Knutson JR, Brand L (1991) The global analysis of fluorescence intensity and anisotropy decay data: second-generation theory and programs. In: Lakowicz JR (ed) *Topics in fluorescence spectroscopy*. Plenum Press, New York, pp 241–306
4. Bevington PR, Robinson KD (2003) *Data reduction and error analysis for the physical sciences*. McGraw-Hill Higher Education, USA

5. Carrazana J, Reija B, Ramos Cabrer P, Al-Soufi W, Novo M, Vázquez Tato J (2004) Complexation of methyl orange with beta-cyclodextrin: detailed analysis and application to quantification of polymer-bound cyclodextrin. *Supramol Chem* 16:549–559
6. Dommelen LV, Boens N, Ameloot M, De Schryver FC, Kowalczyk A (1993) Species-associated spectra and upper and lower bounds on the rate constants of reversible intramolecular two-state excited-state processes with added quencher. global compartmental analysis of the fluorescence decay surface. *J Phys Chem* 97:11738–11753
7. Draper NR, Smith H (1998) *Applied regression analysis*. Wiley, New York
8. Durbin J, Watson GS (1950) Testing for serial correlation in least squares regression. *I. Biometrika* 37:409
9. Dyson RM, Kaderli S, Lawrance GA, Maeder M, Zuberbühler AD (1997) Second order global analysis: the evaluation of series of spectrophotometric titrations for improved determination of equilibrium constants. *Anal Chim Acta* 353:381–393
10. Hamilton JC, Gempferline PJ (1990) Mixture analysis using factor analysis. II: self-modeling curve resolution. *J Chemom* 4:1–13
11. Johnson ML (2000) Parameter correlations while curve fitting. *Methods Enzymol* 321:424–446
12. Jolliffe IT (2002) *Principal component analysis*. Springer, New York
13. Knutson JR, Beechem JM, Brand L (1983) Simultaneous analysis of multiple fluorescence decay curves: a global approach. *Chem Phys Lett* 102:501–507
14. Lawton WH, Sylvestre EA (1971) Elimination of linear parameters in nonlinear regression. *Technometrics* 13:461–467
15. Lezcano M, Al-Soufi W, Novo M, Rodríguez-Núñez E, Vázquez Tato J (2002) Complexation of several benzimidazole-type fungicides with α - and β -cyclodextrins. *J Agric Food Chem* 50:108–112
16. Malinowski ER (1996) Automatic window factor analysis- a more efficient method for determining concentration profiles from evolutionary spectra. *J Chemom* 10:273–279
17. Malinowski ER (2002) *Factor analysis in chemistry*. Wiley, New York
18. Mosquera M, Penedo JC, Ríos Rodríguez MC, Rodríguez-Prieto F (1996) Photoinduced inter- and intramolecular proton transfer in aqueous and ethanolic solutions of 2-(2'-hydroxyphenyl) benzimidazole: evidence for tautomeric and conformational equilibria in the ground state. *J Phys Chem* 100:5398–5407
19. Penedo JC, Ríos Rodríguez MC, García Lema I, Pérez Lustres JL, Mosquera M, Rodríguez-Prieto F (2005) Two competitive routes in the lactim-lactam phototautomerization of a hydroxypyridine derivative cation in water: dissociative mechanism versus water-assisted proton transfer. *J Phys Chem A* 109:10189–10198
20. Penedo JC, Pérez-Lustres JL, Lema García I, Ríos Rodríguez MC, Mosquera M, Rodríguez-Prieto F (2004) Solvent-dependent ground- and excited-state tautomerism in 2-(6'-hydroxy-2'-pyridyl)benzimidazole. *J Phys Chem A* 108:6117–6126
21. Press WH, Teukolsky SA, Vetterling WT, Flannery BP (2002) *Numerical recipes in C++: the art of scientific computing*. Cambridge University Press, New York
22. Puxty G, Maeder M, Hungerbühler K (2006) Tutorial on the fitting of kinetics models to multivariate spectroscopic measurements with non-linear least-squares regression. *Chemom Intell Lab Syst* 81:149–164
23. Reija B, Al-Soufi W, Novo M, Vázquez Tato J (2005) Specific interactions in the inclusion complexes of pyronines Y and B with β -cyclodextrin. *J Phys Chem B* 109:1364–1370
24. Rurack K, Hoffmann K, Al-Soufi W, Resch-Genger U (2002) 2,2'-Bipyridyl-3,3'-diol incorporated into AlPO₄-5 crystals and its spectroscopic properties as related to aqueous liquid media. *J Phys Chem B* 106:9744–9752
25. Sun Y-P, Sears DF Jr, Saltiel J (1988) Principal component self-modeling analysis applied to conformational equilibration of 1,3-butadiene vapor. UV spectra and thermodynamic parameters of the two conformers. *J Am Chem Soc* 110:6277–6278

26. Sylvestre EA, Lawton WH, Maggio MS (1974) Curve resolution using a postulated chemical reaction. *Technometrics* 16:353–368
27. van Stokkum IHM, Larsen DS, van Grondelle R (2004) Global and target analysis of time-resolved spectra. *Biochim Biophys Acta BBA Bioenerg* 1657:82–104
28. Volkov VV (1996) Separation of additive mixture spectra by a self-modeling method. *Appl Spectrosc* 50:320–326
29. Windig W (1992) Self-modeling mixture analysis of spectral data with continuous concentration profiles. *Chemom Intell Lab Syst* 16:1–16

Reviews in Fluorescence 2009

Geddes, C.D. (Ed.)

2011, XII, 392 p., Hardcover

ISBN: 978-1-4419-9671-8